Field Theory Investigation of High-T_c Superconducting Coplanar Waveguide Transmission Lines and Resonators

Jochen Kessler, Roland Dill, and Peter Russer, *Senior Member, IEEE*

Abstract—**We investigate a coplanar waveguide structure using a partial wave synthesis. By this we take into account the complex conductivity of the high-T_c superconductor material according to the two-fluid model and the London theory. Micrometer transmission line dimensions are considered in the frequency range up to 100 GHz suitable e.g. for low-loss, low-dispersion chip-to-chip interconnects. The results obtained for superconductors are also compared with the results for normal conductors with real conductivity and the same geometry. Finally we calculate the behavior of measured and published coplanar waveguide $\lambda/2$ resonators made of high-T_c superconducting thin films [1], [2].**

I. Introduction

THE coplanar transmission line shown in Fig. 1 will eventually be established in more and more applications of microwave integrated circuits. The advantage it confers of avoiding via holes makes it competitive with the widely used microstrip elements [3]. In our consideration of high-T_c superconductor applications, it is an important technological advantage that a ground layer metallization is not needed at the back side of the substrate for this type of transmission line. Coplanar lines allow the realization of small transverse line structures with a single metallization layer and without thinning of the substrates.

II. Analysis of Coplanar Waveguide

For the analysis of the coplanar waveguide (Fig. 1) with finite conductor thickness and complex conductivity, we choose a partial wave synthesis [4], [5]. We consider the structure of Fig. 1 to be embedded in a rectangular hollow waveguide with walls of an ideal conductor. The coplanar waveguide mode, which we are interested in, is an even mode. We can introduce a magnetic wall in the symmetry plane of the structure and therefore we only have to consider one half of the structure. The even

Manuscript received October 22, 1990.

J. Kessler and P. Russer are with the Technical University of Munich, 8000 Munich 2, Germany.

R. Dill is with Siemens AG, Corporate Research and Development, Munich, Germany.

IEEE Log Number 9101127.

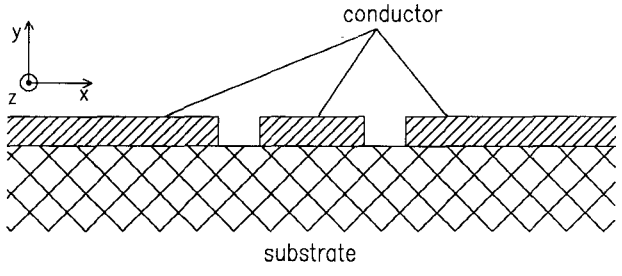

Fig. 1. Coplanar waveguide structure.

symmetric field components result from

$$E_x(-x:y:z) = -E_x(x:y:z) \tag{1a}$$

$$E_y(-x:y:z) = E_y(x:y:z) \tag{1b}$$

$$E_z(-x:y:z) = E_z(x:y:z) \tag{1c}$$

$$H_x(-x:y:z) = H_x(x:y:z) \tag{1d}$$

$$H_y(-x:y:z) = -H_y(x:y:z) \tag{1e}$$

$$H_z(-x:y:z) = -H_z(x:y:z). \tag{1f}$$

Fig. 2 shows the cross section of the waveguide, where the considered right half is divided into five rectangular regions (1 to 5) and three layers (I to III). Each of the regions is assumed to be filled with homogeneous and isotropic material. Since the electrical properties of the superconductor are isotropic within the xz plane and the tangential magnetic field components are dominant, the superconducting regions are assumed to be isotropic in our calculations. The material in each region is commonly described by ϵ and μ, where ϵ results from the relative dielectric constant, ϵ_r, and the complex conductivity, σ_s (as declared in Section III of this paper):

$$\epsilon = \epsilon_0 \epsilon_r + \frac{\sigma_s}{j\omega}. \tag{2}$$

The electric and magnetic fields in each region are, without restriction of generality, described by the so-called

0018-9480/91/0900-1566$01.00 ©1991 IEEE

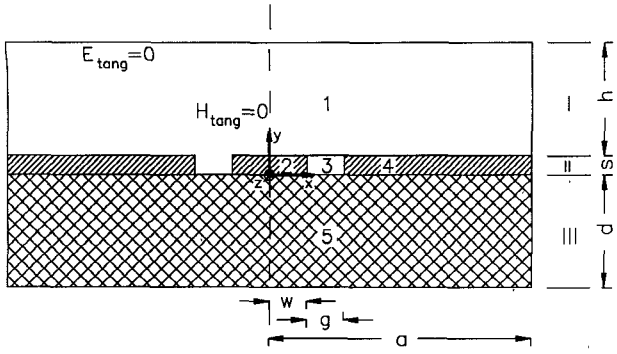

Fig. 2. Cross section of the coplanar structure with regions and layers.

electric and magnetic longitudinal section waves in the x direction (LSE_x and LSH_x), which result from a Hertz vector consisting only of an x component. The Helmholtz equations for these waves are

$$\Delta\Pi_x + \omega^2\mu\epsilon\Pi_x = 0 \qquad (LSE_x \text{ waves}) \tag{3a}$$

$$\Delta\tilde{\Pi}_x + \omega^2\mu\epsilon\tilde{\Pi}_x = 0 \qquad (LSH_x \text{ waves}). \tag{3b}$$

Each field component results from a superposition of LSE_x waves and LSH_x waves:

$$E_x = \frac{\partial^2\Pi_x}{\partial x^2} + \omega^2\mu\epsilon\Pi_x \tag{4a}$$

$$E_y = \frac{\partial^2\Pi_x}{\partial x\,\partial y} - j\omega\mu\frac{\partial\tilde{\Pi}_x}{\partial z} \tag{4b}$$

$$E_z = \frac{\partial^2\Pi_x}{\partial x\,\partial z} + j\omega\mu\frac{\partial\tilde{\Pi}_x}{\partial y} \tag{4c}$$

$$H_x = \frac{\partial^2\tilde{\Pi}_x}{\partial x^2} + \omega^2\mu\epsilon\tilde{\Pi}_x \tag{4d}$$

$$H_y = j\omega\epsilon\frac{\partial\Pi_x}{\partial z} + \frac{\partial^2\tilde{\Pi}_x}{\partial x\,\partial y} \tag{4e}$$

$$H_z = -j\omega\epsilon\frac{\partial\Pi_x}{\partial y} + \frac{\partial^2\tilde{\Pi}_x}{\partial x\,\partial z}. \tag{4f}$$

For a wave propagating in the $+z$ direction, the Hertz vectors of the LSE_x and LSH_x waves are

$$\Pi_x = \sum_m \left\{\left(A_m e^{jk_{xm}x} + B_m e^{-jk_{xm}x}\right)\cdot\left(C_m e^{jk_{ym}y} + D_m e^{-jk_{ym}y}\right)\right\} e^{j(\omega t - k_z z)} \tag{5a}$$

$$\tilde{\Pi}_x = \sum_m \left\{\left(\tilde{A}_m e^{j\tilde{k}_{xm}x} + \tilde{B}_m e^{-j\tilde{k}_{xm}x}\right)\cdot\left(\tilde{C}_m e^{j\tilde{k}_{ym}y} + \tilde{D}_m e^{-j\tilde{k}_{ym}y}\right)\right\} e^{j(\omega t - k_z z)}. \tag{5b}$$

In the following, the factor $e^{j(\omega t - k_z z)}$, which is the same for all elements of the series, is suppressed. From (4a)–(4f) and (5) we obtain the following field components:

$$E_x = \sum_m \left\{\left(k^2 - k_{xm}^2\right)\left(A_m e^{jk_{xm}x} + B_m e^{-jk_{xm}x}\right)\cdot\left(C_m e^{jk_{ym}y} + D_m e^{-jk_{ym}y}\right)\right\} \tag{6a}$$

$$E_y = \sum_m \left\{-k_{xm}k_{ym}\left(A_m e^{jk_{xm}x} - B_m e^{-jk_{xm}x}\right)\cdot\left(C_m e^{jk_{ym}y} - D_m e^{-jk_{ym}y}\right) - \omega\mu k_z\left(\tilde{A}_m e^{j\tilde{k}_{xm}x} + \tilde{B}_m e^{-j\tilde{k}_{xm}x}\right)\cdot\left(\tilde{C}_m e^{j\tilde{k}_{ym}y} + \tilde{D}_m e^{-j\tilde{k}_{ym}y}\right)\right\} \tag{6b}$$

$$E_z = \sum_m \left\{k_{xm}k_z\left(A_m e^{jk_{xm}x} - B_m e^{-jk_{xm}x}\right)\cdot\left(C_m e^{jk_{ym}y} + D_m e^{-jk_{ym}y}\right) - \omega\mu k_{ym}\left(\tilde{A}_m e^{j\tilde{k}_{xm}x} + \tilde{B}_m e^{-j\tilde{k}_{xm}x}\right)\cdot\left(\tilde{C}_m e^{j\tilde{k}_{ym}y} - \tilde{D}_m e^{-j\tilde{k}_{ym}y}\right)\right\} \tag{6c}$$

$$H_x = \sum_m \left\{\left(k^2 - k_{xm}^2\right)\left(\tilde{A}_m e^{j\tilde{k}_{xm}x} + \tilde{B}_m e^{-j\tilde{k}_{xm}x}\right)\cdot\left(\tilde{C}_m e^{j\tilde{k}_{ym}y} + \tilde{D}_m e^{-j\tilde{k}_{ym}y}\right)\right\} \tag{6d}$$

$$H_y = \sum_m \left\{\omega\epsilon k_z\left(A_m e^{jk_{xm}x} + B_m e^{-jk_{xm}x}\right)\cdot\left(C_m e^{jk_{ym}y} + D_m e^{-jk_{ym}y}\right) - k_{xm}k_{ym}\left(\tilde{A}_m e^{j\tilde{k}_{xm}x} - \tilde{B}_m e^{-j\tilde{k}_{xm}x}\right)\cdot\left(\tilde{C}_m e^{j\tilde{k}_{ym}y} - \tilde{D}_m e^{-j\tilde{k}_{ym}y}\right)\right\} \tag{6e}$$

$$H_z = \sum_m \left\{\omega\epsilon k_{ym}\left(A_m e^{jk_{xm}x} + B_m e^{-jk_{xm}x}\right)\cdot\left(C_m e^{jk_{ym}y} - D_m e^{-jk_{ym}y}\right) + k_{xm}k_z\left(\tilde{A}_m e^{j\tilde{k}_{xm}x} - \tilde{B}_m e^{-j\tilde{k}_{xm}x}\right)\cdot\left(\tilde{C}_m e^{j\tilde{k}_{ym}y} + \tilde{D}_m e^{-j\tilde{k}_{ym}y}\right)\right\}. \tag{6f}$$

For regions 1 and 5 (Fig. 2) we have three homogeneous boundary conditions for the tangential electric and magnetic fields:

$$H_y(x=0) = 0 \qquad H_z(x=0) = 0 \tag{7a}$$

$$E_y(x=a) = 0 \qquad E_z(x=a) = 0 \tag{7b}$$

$$E_x(y=y_0) = 0 \qquad E_z(y=y_0) = 0 \tag{7c}$$

where $y_0 = s + h$ for region 1 and $y_0 = -d$ for region 5. Including these boundary conditions in (6), we get the

following simplification for the regions $i = 1$ and 5:

$$E_{ix} = \sum_m \left\{ \left[-A_{\iota m}\left(k_i^2 - k_{15xm}^2\right)\right] \sin\left[k_{15xm}x\right] \cdot \sin\left[k_{iym}(y - y_{0i})\right]\right\} \tag{8a}$$

$$E_{\iota y} = \sum_m \left\{ \left[-A_{\iota m}k_{15xm}k_{iym} - \tilde{A}_{\iota m}\omega\mu_\iota k_z\right] \cdot \cos\left[k_{15xm}x\right]\cos\left[k_{\iota ym}(y - y_{0\iota})\right]\right\} \tag{8b}$$

$$E_{\iota z} = \sum_m \left\{ \left[jA_{\iota m}k_{15xm}k_z - j\tilde{A}_{im}\omega\mu_\iota k_{\iota ym}\right] \cdot \cos\left[k_{15xm}x\right]\sin\left[k_{iym}(y - y_{0\iota})\right]\right\} \tag{8c}$$

$$H_{\iota x} = \sum_m \left\{ \left[\tilde{A}_{\iota m}\left(k_i^2 - k_{15xm}^2\right)\right] \cos\left[k_{15xm}x\right] \cdot \cos\left[k_{\iota ym}(y - y_{0i})\right]\right\} \tag{8d}$$

$$H_{\iota y} = \sum_m \left\{ \left[-A_{\iota m}\omega\epsilon_\iota k_z + \tilde{A}_{\iota m}k_{15xm}k_{\iota ym}\right] \cdot \sin\left[k_{15xm}x\right]\sin\left[k_{\iota ym}(y - y_{0\iota})\right]\right\} \tag{8e}$$

$$H_{iz} = \sum_m \left\{ \left[jA_{\iota m}\omega\epsilon_i k_{\iota ym} + j\tilde{A}_{\iota m}k_{15xm}k_z\right] \cdot \sin\left[k_{15xm}x\right]\cos\left[k_{\iota ym}(y - y_{0\iota})\right]\right\} \tag{8f}$$

where

$$k_{15xm} = (m - 0.5)\frac{\pi}{a} \tag{8g}$$

and

$$y_{01} = s + h \qquad y_{05} = -d. \tag{8h}$$

The boundary condition of (7a) also concerns region 2, for which we obtain

$$E_{2x} = \sum_m \left\{ \left(k_2^2 - k_{2xm}^2\right) jA_{2m}\sin\left[k_{2xm}x\right] \cdot \left[e^{jk_{2ym}y} + B_{2m}e^{-jk_{2ym}y}\right]\right\} \tag{9a}$$

$$E_{2y} = \sum_m \left\{ -k_{2xm}k_{2ym}A_{2m}\cos\left[k_{2xm}x\right] \cdot \left[e^{jk_{2ym}y} - B_{2m}e^{-jk_{2ym}y}\right] - \omega\mu_2 k_z\tilde{A}_{2m} \cdot \cos\left[\tilde{k}_{2xm}x\right]\left[e^{j\tilde{k}_{2ym}y} + \tilde{B}_{2m}e^{-j\tilde{k}_{ym}y}\right]\right\} \tag{9b}$$

$$E_{2z} = \sum_m \left\{ k_{2xm}k_z A_{2m}\cos\left[k_{2xm}x\right] \cdot \left[e^{jk_{2ym}y} - B_{2m}e^{-jk_{2ym}y}\right] - \omega\mu_2\tilde{k}_{2ym}\tilde{A}_{2m} \cdot \cos\left[\tilde{k}_{2\chi m}x\right]\left[e^{j\tilde{k}_{2ym}y} - \tilde{B}_{2m}e^{-j\tilde{k}_{2ym}y}\right]\right\} \tag{9c}$$

$$H_{2x} = \sum_m \left\{ \left(k_2^2 - \tilde{k}_{2xm}^2\right)\tilde{A}_{2m}\cos\left[\tilde{k}_{2xm}x\right] \cdot \left[e^{j\tilde{k}_{2ym}y} + \tilde{B}_{2m}e^{-j\tilde{k}_{2\nu m}y}\right]\right\} \tag{9d}$$

$$H_{2y} = \sum_m \left\{ \omega\epsilon_2 k_z jA_{2m}\sin\left[k_{2xm}x\right] \cdot \left[e^{jk_{2ym}y} + B_{2m}e^{-jk_{2ym}y}\right] - \tilde{k}_{2xm}\tilde{k}_{2ym}j\tilde{A}_{2m}\sin\left[\tilde{k}_{2xm}x\right] \cdot \left[e^{j\tilde{k}_{2\nu m}y} - \tilde{B}_{2m}e^{-j\tilde{k}_{2ym}y}\right]\right\} \tag{9e}$$

$$H_{2z} = \sum_m \left\{ \omega\epsilon_2 k_{2ym}jA_{2m}\sin\left[k_{2xm}x\right] \cdot \left[e^{jk_{2ym}y} - B_{2m}e^{-jk_{2ym}y}\right] + \tilde{k}_{2xm}k_z j\tilde{A}_{2m}\sin\left[\tilde{k}_{2xm}x\right] \cdot \left[e^{j\tilde{k}_{2\nu m}y} + \tilde{B}_{2m}e^{-j\tilde{k}_{2ym}y}\right]\right\}. \tag{9f}$$

For region 3, the boundary conditions of (7) are not relevant. So we can eliminate only two coefficients from the general equation (6) and then obtain

$$E_{3x} = \sum_m \left\{ \left(k_3^2 - k_{3xm}^2\right)A_{3m}\left[e^{jk_{3xm}x} + B_{3m}e^{-jk_{3xm}x}\right] \cdot \left[e^{jk_{3ym}y} + C_{3m}e^{-jk_{3ym}y}\right]\right\} \tag{10a}$$

$$E_{3y} = \sum_m \left\{ -k_{3xm}k_{3ym}A_{3m}\left[e^{jk_{3\chi m}x} - B_{3m}e^{-jk_{3xm}x}\right] \cdot \left[e^{jk_{3\nu m}y} - C_{3m}e^{-jk_{3ym}y}\right] - \omega\mu_3 k_z\tilde{A}_{3m}\left[e^{j\tilde{k}_{3\nu m}x} + \tilde{B}_{3m}e^{-j\tilde{k}_{3xm}x}\right] \cdot \left[e^{j\tilde{k}_{3\nu m}y} + \tilde{C}_{3m}e^{-j\tilde{k}_{3ym}y}\right]\right\} \tag{10b}$$

$$E_{3z} = \sum_m \left\{ k_{3xm}k_z A_{3m}\left[e^{jk_{3xm}x} - B_{3m}e^{-jk_{3xm}x}\right] \cdot \left[e^{jk_{3ym}y} + C_{3m}e^{-jk_{3ym}y}\right] - \omega\mu_3\tilde{k}_{3ym}\tilde{A}_{3m}\left[e^{j\tilde{k}_{3\nu m}x} + \tilde{B}_{3m}e^{-j\tilde{k}_{3xm}x}\right] \cdot \left[e^{j\tilde{k}_{3\nu m}y} - \tilde{C}_{3m}e^{-j\tilde{k}_{3ym}y}\right]\right\} \tag{10c}$$

$$H_{3x} = \sum_m \left\{ \left(k_3^2 - \tilde{k}_{3xm}^2\right)\tilde{A}_{3m}\left[e^{j\tilde{k}_{3xm}x} + \tilde{B}_{3m}e^{-j\tilde{k}_{3xm}x}\right] \cdot \left[e^{j\tilde{k}_{3ym}y} + \tilde{C}_{3m}e^{-j\tilde{k}_{3ym}y}\right]\right\} \tag{10d}$$

$$H_{3y} = \sum_m \left\{ \omega\epsilon_3 k_z A_{3m}\left[e^{jk_{3xm}x} + B_{3m}e^{-jk_{3xm}x}\right] \cdot \left[e^{jk_{3ym}y} + C_{3m}e^{-jk_{3ym}y}\right] - \tilde{k}_{3xm}\tilde{k}_{3ym}\tilde{A}_{3m}\left[e^{j\tilde{k}_{3xm}x} - \tilde{B}_{3m}e^{-j\tilde{k}_{3xm}x}\right] \cdot \left[e^{j\tilde{k}_{3\nu m}y} - \tilde{C}_{3m}e^{-j\tilde{k}_{3ym}y}\right]\right\} \tag{10e}$$

$$H_{3z} = \sum_m \left\{ \omega\epsilon_3 k_{3ym}A_{3m}\left[e^{jk_{3xm}x} + B_{3m}e^{-jk_{3xm}x}\right] \cdot \left[e^{jk_{3ym}y} - C_{3m}e^{-jk_{3ym}y}\right] + \tilde{k}_{3xm}k_z\tilde{A}_{3m}\left[e^{j\tilde{k}_{3xm}x} - \tilde{B}_{3m}e^{-j\tilde{k}_{3xm}x}\right] \cdot \left[e^{j\tilde{k}_{3ym}y} + \tilde{C}_{3m}e^{-j\tilde{k}_{3ym}y}\right]\right\}. \tag{10f}$$

For the remaining region 4, we take into account the boundary condition of (7b) and obtain the following approach:

$$E_{4x} = \sum_m \left\{ (k_4^2 - k_{4xm}^2) A_{4m} \cos\left[k_{4xm}(x-a)\right] \cdot \left[e^{jk_{4ym}y} + B_{4m} e^{-jk_{4ym}y}\right] \right\} \tag{11a}$$

$$E_{4y} = \sum_m \Big\{ -k_{4xm} k_{4ym} j A_{4m} \sin\left[k_{4xm}(x-a)\right] \cdot \left[e^{jk_{4ym}y} - B_{4m} e^{-jk_{4ym}y}\right] - \omega\mu_4 k_z j \tilde{A}_{4m} \sin\left[\tilde{k}_{4xm}(x-a)\right] \cdot \left[e^{j\tilde{k}_{4ym}y} + \tilde{B}_{4m} e^{-j\tilde{k}_{4ym}y}\right] \Big\} \tag{11b}$$

$$E_{4z} = \sum_m \Big\{ k_{4xm} k_z j A_{4m} \sin\left[k_{4xm}(x-a)\right] \cdot \left[e^{jk_{4ym}y} + B_{4m} e^{-jk_{4ym}y}\right] - \omega\mu_4 \tilde{k}_{4ym} j \tilde{A}_{4m} \sin\left[\tilde{k}_{4xm}(x-a)\right] \cdot \left[e^{j\tilde{k}_{4ym}y} - \tilde{B}_{4m} e^{-j\tilde{k}_{4ym}y}\right] \Big\} \tag{11c}$$

$$H_{4x} = \sum_m \left\{ (k_4^2 - \tilde{k}_{4xm}^2) j \tilde{A}_{4m} \sin\left[\tilde{k}_{4xm}(x-a)\right] \cdot \left[e^{j\tilde{k}_{4ym}y} + \tilde{B}_{4m} e^{-j\tilde{k}_{4ym}y}\right] \right\} \tag{11d}$$

$$H_{4y} = \sum_m \Big\{ \omega\epsilon_4 k_z A_{4m} \cos\left[k_{4xm}(x-a)\right] \cdot \left[e^{jk_{4ym}y} + B_{4m} e^{-jk_{4ym}y}\right] - \tilde{k}_{4xm} \tilde{k}_{4ym} \tilde{A}_{4m} \cos\left[\tilde{k}_{4xm}(x-a)\right] \cdot \left[e^{j\tilde{k}_{4ym}y} - \tilde{B}_{4m} e^{-j\tilde{k}_{4ym}y}\right] \Big\} \tag{11e}$$

$$H_{4z} = \sum_m \Big\{ \omega\epsilon_4 k_{4ym} A_{4m} \cos\left[k_{4xm}(x-a)\right] \cdot \left[e^{jk_{4ym}y} - B_{4m} e^{-jk_{4ym}y}\right] + \tilde{k}_{4xm} k_z \tilde{A}_{4m} \cos\left[\tilde{k}_{4xm}(x-a)\right] \cdot \left[e^{j\tilde{k}_{4ym}y} + \tilde{B}_{4m} e^{-j\tilde{k}_{4ym}y}\right] \Big\}. \tag{11f}$$

Now we have to match the tangential field components at the vertical boundaries in layer II between regions 2, 3, and 4:

$$E_{2y}(x=w) = E_{3y}(x=w) \tag{12a}$$

$$E_{2z}(x=w) = E_{3z}(x=w) \tag{12b}$$

$$H_{2y}(x=w) = H_{3y}(x=w) \tag{12c}$$

$$H_{2z}(x=w) = H_{3z}(x=w) \tag{12d}$$

$$E_{3y}(x=w+g) = E_{4y}(x=w+g) \tag{12e}$$

$$E_{3z}(x=w+g) = E_{4z}(x=w+g) \tag{12f}$$

$$H_{3y}(x=w+g) = H_{4y}(x=w+g) \tag{12g}$$

$$H_{3z}(x=w+g) = H_{4z}(x=w+g). \tag{12h}$$

$$\forall y \in [0,s].$$

In order to fulfill (12) for each series element m and for LSE_x waves and LSH_x waves $\forall y \in [0,s]$ separately, we define

$$B_{\mathrm{II}m} := B_{2m} = C_{3m} = B_{4m} \tag{13a}$$

$$\tilde{B}_{\mathrm{II}m} := \tilde{B}_{2m} = \tilde{C}_{3m} = \tilde{B}_{4m} \tag{13b}$$

$$k_{\mathrm{II}ym} := k_{2ym} = k_{3ym} = k_{4ym} \tag{14a}$$

$$\tilde{k}_{\mathrm{II}ym} := \tilde{k}_{2ym} = \tilde{k}_{3ym} = \tilde{k}_{4ym}. \tag{14b}$$

In this way we get the same dependence in the y direction for each series element of the regions in layer II. From (9) to (14) we obtain the following conditions for a continual transition of the tangential field components at the vertical boundaries in layer II:

$$k_{2xm} A_{2m} \cos\left[k_{2xm} w\right] = k_{3xm} A_{3m} \left[e^{jk_{3xm}w} - B_{3m} e^{-jk_{3xm}w}\right] \tag{15a}$$

$$j\epsilon_2 A_{2m} \sin\left[k_{2xm} w\right] = \epsilon_3 A_{3m} \left[e^{jk_{3xm}w} + B_{3m} e^{-jk_{3xm}w}\right] \tag{15b}$$

$$k_{3xm} A_{3m} \left[e^{jk_{3xm}(w+g)} - B_{3m} e^{-jk_{3xm}(w+g)}\right] = jk_{4xm} A_{4m} \sin\left[k_{4xm}(w+g-a)\right] \tag{15c}$$

$$\epsilon_3 A_{3m} \left[e^{jk_{3xm}(w+g)} + B_{3m} e^{-jk_{3xm}(w+g)}\right] = \epsilon_4 A_{4m} \cos\left[k_{4xm}(w+g-a)\right] \tag{15d}$$

for LSE_x waves and

$$x\epsilon_3 A_{3m} \left[e^{jk_{3xm}(w+g)} + B_{3m} e^{-jk_{3xm}(w+g)}\right] \mu_2 \tilde{A}_{2m} \cos\left[\tilde{k}_{2xm} w\right] = \mu_3 \tilde{A}_{3m} \left[e^{j\tilde{k}_{3xm}w} + \tilde{B}_{3m} e^{-j\tilde{k}_{3xm}w}\right] \tag{16a}$$

$$j\tilde{k}_{2xm} \tilde{A}_{2m} \sin\left[\tilde{k}_{2xm} w\right] = \tilde{k}_{3xm} \tilde{A}_{3m} \left[e^{j\tilde{k}_{3xm}w} - \tilde{B}_{3m} e^{-j\tilde{k}_{3xm}w}\right] \tag{16b}$$

$$\mu_3 \tilde{A}_{3m} \left[e^{j\tilde{k}_{3xm}(w+g)} + \tilde{B}_{3m} e^{-j\tilde{k}_{3xm}(w+g)}\right] = j\mu_4 \tilde{A}_{4m} \sin\left[\tilde{k}_{4xm}(w+g-a)\right] \tag{16c}$$

$$\tilde{k}_{3xm} \tilde{A}_{3m} \left[e^{j\tilde{k}_{3xm}(w+g)} - \tilde{B}_{3m} e^{-j\tilde{k}_{3xm}(w+g)}\right] = \tilde{k}_{4xm} \tilde{A}_{4m} \cos\left[\tilde{k}_{4xm}(w+g-a)\right] \tag{16d}$$

for LSH_x waves. The wavenumbers in the x direction, $k_{2xm}, k_{3xm}, k_{4xm}$ and $\tilde{k}_{2xm}, \tilde{k}_{3xm}, \tilde{k}_{4xm}$, have to be determined by (15) and (16) so that they have a nontrivial solution with respect to the linear system with the unknown coefficients A_{2m}, A_{3m}, $A_{3m}B_{3m}$, A_{4m}, and $\tilde{A}_{2m}, \tilde{A}_{3m}, \tilde{A}_{3m}\tilde{B}_{3m}, \tilde{A}_{4m}$. In addition the following relations between the wavenumbers k_{ixm} and $\tilde{k}_{ixm}$ in the different regions of layer II must be fulfilled:

$$k_{ixm}^2 = k_{jxm}^2 + k_i^2 - k_j^2, \qquad i,j = 2,3,4 \tag{17a}$$

$$\tilde{k}_{ixm}^2 = \tilde{k}_{jxm}^2 + k_i^2 - k_j^2, \qquad i,j = 2,3,4 \tag{17b}$$

because (14) and

$$k_i^2 = \omega^2 \mu_i \epsilon_i = k_{ixm}^2 + k_{iym}^2 + k_z^2 = \tilde{k}_{ixm}^2 + \tilde{k}_{iym}^2 + k_z^2. \tag{18}$$

The remaining boundary conditions are the continuity of the tangential field components at the boundaries between the layers (boundary I/II: $i=1$, $y=s$; boundary III/II: $i=5$, $y=0$):

$$E_{ix} = E_{2x}\ \forall x \in [0,w] \qquad E_{ix} = E_{3x}\ \forall x \in [w,w+g] \qquad E_{ix} = E_{4x}\ \forall x \in [w+g,a] \tag{19a}$$

$$E_{iz} = E_{2z}\ \forall x \in [0,w] \qquad E_{iz} = E_{3z}\ \forall x \in [w,w+g] \qquad E_{iz} = E_{4z}\ \forall x \in [w+g,a] \tag{19b}$$

$$H_{ix} = H_{2x}\ \forall x \in [0,w] \qquad H_{ix} = H_{3x}\ \forall x \in [w,w+g] \qquad H_{ix} = H_{4x}\ \forall x \in [w+g,a] \tag{19c}$$

$$H_{iz} = H_{2z}\ \forall x \in [0,w] \qquad H_{iz} = H_{3z}\ \forall x \in [w,w+g] \qquad H_{iz} = H_{4z}\ \forall x \in [w+g,a] \tag{19d}$$

For matching the tangential field components at the horizontal boundaries $y=s$ and $y=0$, we use the moment method. The test functions which are applied to the orthogonal series of (8) to (11) are the functions of (8) at $y=$ constant itself. Thus we get certain diagonal submatrices in the resulting system of equations:

$$\begin{bmatrix} D_1 & 0 & M_1 & 0 & M_2 & 0 & 0 & 0 \\ D_2 & D_3 & M_3 & M_4 & M_5 & M_6 & 0 & 0 \\ 0 & D_4 & 0 & M_7 & 0 & M_8 & 0 & 0 \\ D_5 & D_6 & M_9 & M_{10} & M_{11} & M_{12} & 0 & 0 \\ 0 & 0 & M_{13} & 0 & M_{13} & 0 & D_7 & 0 \\ 0 & 0 & M_{14} & M_{15} & M_{14} & -M_{15} & D_8 & D_9 \\ 0 & 0 & 0 & M_{16} & 0 & M_{16} & 0 & D_{10} \\ 0 & 0 & M_{17} & M_{18} & -M_{17} & M_{18} & D_{11} & D_{12} \end{bmatrix} \cdot \begin{bmatrix} A_{1m} \\ \tilde{A}_{1m} \\ A_{3m} \\ \tilde{A}_{3m} \\ A_{3m}B_{\mathrm{II}m} \\ \tilde{A}_{3m}\tilde{B}_{\mathrm{II}m} \\ A_{5m} \\ \tilde{A}_{5m} \end{bmatrix} = \vec{0} \tag{20}$$

with D_j denoting a diagonal submatrix and M_j a full submatrix. The matrix of (20) can be reduced by eliminating A_{1m}, $\tilde{A}_{1m}$, A_{5m}, and $\tilde{A}_{5m}$. Then we obtain the following system of equations:

$$\begin{bmatrix} M_3 - \frac{D_2}{D_1}M_1 & M_4 - \frac{D_3}{D_4}M_7 & M_5 - \frac{D_2}{D_1}M_2 & M_6 - \frac{D_3}{D_4}M_8 \\ M_9 - \frac{D_5}{D_1}M_1 & M_{10} - \frac{D_6}{D_4}M_7 & M_{11} + \frac{D_5}{D_1}M_2 & M_{12} + \frac{D_6}{D_4}M_8 \\ M_{14} - \frac{D_8}{D_7}M_{13} & M_{15} - \frac{D_9}{D_{10}}M_{16} & M_{14} - \frac{D_8}{D_7}M_{13} & -\left(M_{15} + \frac{D_9}{D_{10}}M_{16}\right) \\ M_{17} - \frac{D_{11}}{D_7}M_{13} & M_{18} - \frac{D_{12}}{D_{10}}M_{16} & -\left(M_{17} + \frac{D_{11}}{D_7}M_{13}\right) & M_{18} - \frac{D_{12}}{D_{10}}M_{16} \end{bmatrix} \cdot \begin{bmatrix} A_{3m} \\ \tilde{A}_{3m} \\ A_{3m}B_{\mathrm{II}m} \\ \tilde{A}_{3m}\tilde{B}_{\mathrm{II}m} \end{bmatrix} = \vec{0} \tag{21}$$

with the back-substitution:

$$A_{1m} = -D_1^{-1}(M_1 A_{3m} + M_2 A_{3m} B\Pi_m) \tag{22a}$$

$$\tilde{A}_{1m} = -D_4^{-1}\left(M_7 \tilde{A}_{3m} + M_8 \tilde{A}_{3m} \tilde{B}\Pi_m\right) \tag{22b}$$

$$A_{5m} = -D_7^{-1} M_{13}(A_{3m} + A_{3m} B_{\mathrm{II}m}) \tag{22c}$$

$$\tilde{A}_{5m} = -D_{10}^{-1} M_{16}\left(\tilde{A}_{3m} + \tilde{A}_{3m}\tilde{B}_{\mathrm{II}m}\right). \tag{22d}$$

Before we can solve (21), which is linear with respect to the coefficients A_{3m}, $\tilde{A}_{3m}$, $A_{3m}B_{\mathrm{II}m}$, and $\tilde{A}_{3m}\tilde{B}_{\mathrm{II}m}$, we must determine k_z, which is a nonlinear problem. A proper starting value is the quasi-static approach for an ideal conductor layer with zero thickness. After computing k_z by iteration, we obtain the unknown wavenumbers in the y direction by (18) and then solve the linear system of equations (21). After the back-substitution (22) we are able to determine all field components in all regions with the help of (8) to (11).

III. Complex Conductivity

We use the London theory to describe local relations between the superconductive current and the correlated electric and magnetic fields [6]. We start from the Maxwell equations

$$\mathrm{rot}\,\vec{H} = \vec{j} + \dot{\vec{D}} \tag{23a}$$

$$\mathrm{rot}\,\vec{E} = -\dot{\vec{B}} \tag{23b}$$

$$\mathrm{div}\,\vec{D} = \rho \tag{23c}$$

$$\mathrm{div}\,\vec{B} = 0 \tag{23d}$$

the material equations

$$\vec{D} = \epsilon_r \epsilon_0 \vec{E} \tag{24a}$$

$$\vec{B} = \mu \vec{H} \tag{24b}$$

and the London equations

$$\mu \lambda_l^2 \dot{\vec{j}}_s = \vec{E} \tag{25a}$$

$$\mathrm{rot}\left(\lambda_l^2 \vec{j}_s\right) = -\vec{H} \tag{25b}$$

where λ_l is the London penetration depth:

$$\lambda_l = \begin{cases} \infty & \forall T > T_c \\ \dfrac{\lambda_{l0}}{\sqrt{1-\left[\dfrac{T}{T_c}\right]^4}} & \forall T < T_c \end{cases} \tag{26}$$

with T_c the critical temperature of the superconductor and λ_{l0} the London penetration depth at $T = 0$.

Common characteristics of normal and superconducting current are as follows:

- The current is proportional to charge density and velocity:

$$\vec{j} = \rho \vec{v}. \tag{27}$$

- The charge driving force is proportional to the electric field:

$$\vec{F} = q\vec{E}. \tag{28}$$

Different characteristics are as follows:

- In the case of normal current the charge driving force is used to compensate "friction losses" proportional to velocity:

$$\vec{F} \sim \vec{v} \Rightarrow \vec{E} \sim \vec{j}_n = \sigma \vec{E}. \tag{29a}$$

- In the case of superconducting current, however, the driving force is used for charge acceleration:

$$\vec{F} \sim \dot{\vec{v}} \Rightarrow \vec{E} \sim \dot{\vec{j}}_s = \frac{1}{\mu \lambda_l^2}\vec{E}. \tag{29b}$$

In the case of superconductivity we obtain from (23a), with $\vec{j} = \vec{j}_n + \vec{j}_s$ and $\partial/\partial t = j\omega$,

$$\operatorname{rot} \vec{H} = \underbrace{\sigma \vec{E}}_{\substack{\text{normally} \\ \text{conducting}}} + \underbrace{\frac{1}{j\omega\mu\lambda_l^2}\vec{E}}_{\substack{\text{super-} \\ \text{conducting}}} + \underbrace{j\omega\epsilon_r\epsilon_0\vec{E}}_{\substack{\text{dielectric} \\ \text{part}}}. \tag{30}$$

We introduce a general complex conductivity, σ_s, so that normal and superconducting current are comprehended in one term:

$$\vec{j} = \vec{j}_n + \vec{j}_s = \sigma_s \vec{E} \tag{31}$$

and obtain for the general conductivity, σ_s,

$$\sigma_s = \sigma + \frac{1}{j\omega\mu\lambda_l^2}. \tag{32}$$

For superconductive materials in the analysis of Section II we have to replace the real conductivity, σ, in (2) with the complex conductivity, σ_s, of (32).

IV. Resonator Structure

Fig. 3 shows the structure of the coplanar waveguide short-circuit $\lambda/2$ resonator capacitively coupled to the lead conductor as measured and published in [1] and [2]. The unloaded Q values, Q_u, of the structure can be obtained from the waveguide analysis assuming ideal short

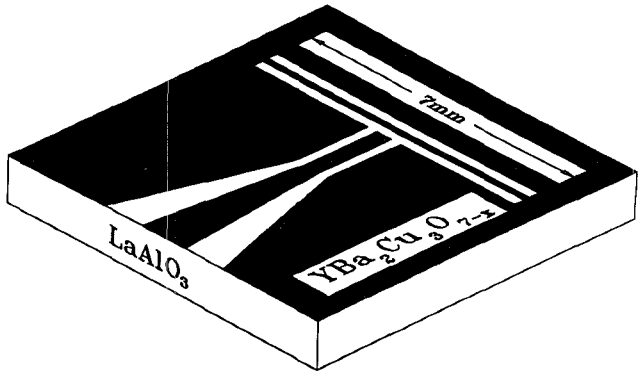

Fig. 3. Resonator structure.

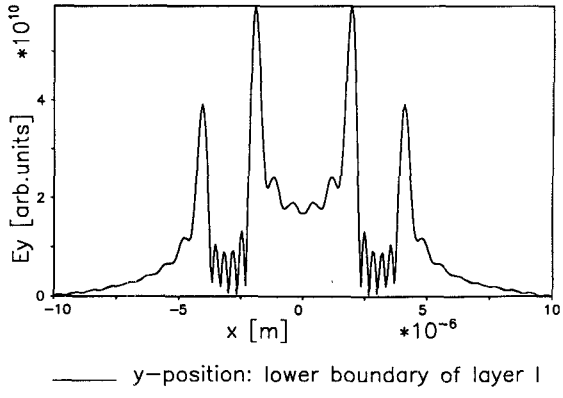

Fig. 4. E_y component without Hamming window.

circuits at both ends of the resonator:

$$Q_u = \frac{2\pi}{(1 - e^{-2\alpha_{\text{res}}\lambda_{\text{res}}})} \tag{33}$$

where $\alpha_{\text{res}} = -\mathcal{I}m\{k_{z\,\text{res}}\}$, $\lambda_{\text{res}} = 2\pi / \mathcal{R}e\{k_{z\,\text{res}}\}$ and $k_{z\,\text{res}}$ is the wavenumber k_z at resonance frequency. For $\alpha_{\text{res}}\lambda_{\text{res}} \ll 1$ one can approach (33) by

$$Q_u = \frac{\beta_{\text{res}}}{2\alpha_{\text{res}}} \tag{34}$$

where $\beta_{\text{res}} = \mathcal{R}e\{k_{z\,\text{res}}\}$.

V. Results

For the presentation of field distributions it is appropriate to weight the coefficients $A_{\iota m}$, $\tilde{A}_{\iota m}$, B_{im}, and $\tilde{B}_{im}$ in (8) to (11) by using a window function, in order to eliminate oscillations caused by breaking off the infinite series at $m = m_0$. A proper window function is the Hamming window [7]:

$$A, B_{im}^{\text{new}} = \left\{0.5 + 0.5\cos\left(\frac{\pi \cdot \mathcal{R}e\{k_{ixm}\}}{\mathcal{R}e\{k_{x\,\max}\}}\right)\right\} A, B_{im} \tag{35}$$

where $k_{x\,\max}$ is the k_{ixm} with the largest account of the real part, $|\mathcal{R}e\{k_{ixm}\}|$.

Fig. 4 shows the distribution of the E_y component upon the conductor layer without the Hamming window, and Fig. 5 shows the distribution with the window.

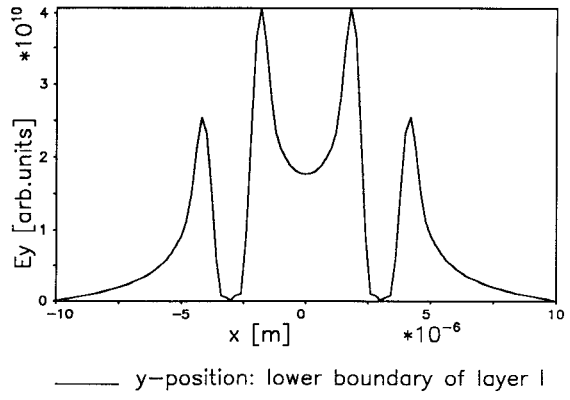

Fig. 5. E_y component with Hamming window.

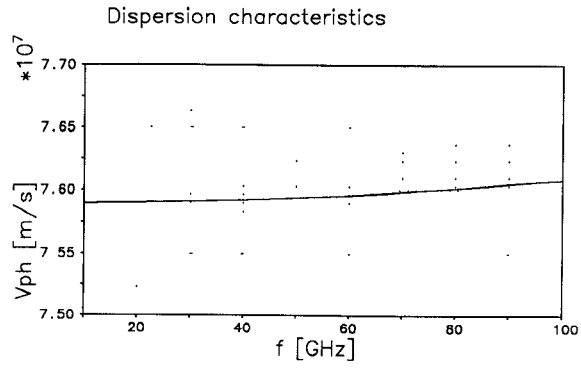

Fig. 7. Phase velocity (superconducting case).

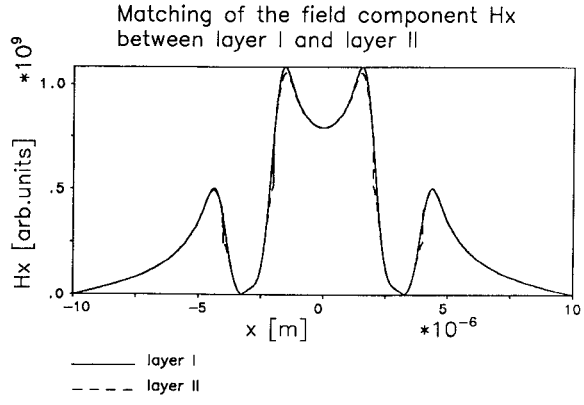

Fig. 6. Matching of the H_x component.

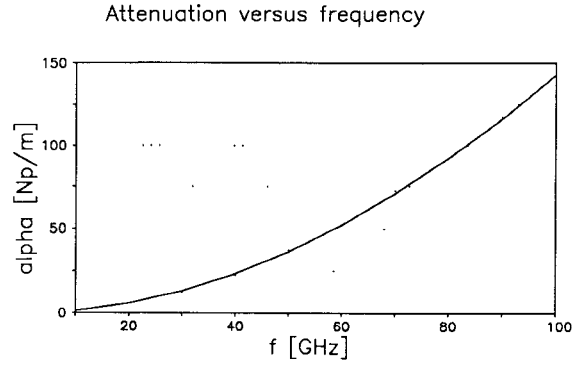

Fig. 8. Attenuation constant (superconducting case).

The following examples are according to a high-T_c coplanar transmission line (see Fig. 2) made by a $YBa_2Cu_3O_{7-x}$ thin film [8] on a $LaAlO_3$ substrate [9]:

width of conductor strip $2w = 4\ \mu$m
gap width $g = 4\ \mu$m
total width $2a = 20\ \mu$m
substrate thickness $d = 0.5$ mm
superconductor thickness $s = 250$ nm
height of superstrate $h = 0.5$ mm
relative dielectric constants $\epsilon_{r1,3} = 1$, $\epsilon_{r2,4} = 0$, $\epsilon_{r5} = 24$
normal conductivities (77 K) $\sigma_{1,3} = 0$, $\sigma_{2,4} = 4 \cdot 10^6$ S/m, $\sigma_5 = 1.1 \cdot 10^{-3}$ S/m
London penetration depths (77 K) $\lambda_{l1,3} \to \infty$, $\lambda_{l2,4} =$ 240 nm, $\lambda_{l5} \to \infty$.

Fig. 6 presents the matching of the H_x component at the boundary between layer I and layer II at 10 GHz. The solid line describes layer I and the dashed line, layer II.

Fig. 7 shows the phase velocity $v_{ph} = \omega/\beta$ versus frequency in the range from 10 to 100 GHz. No significant variations occur in the observed frequency range. The phase velocity varies only 0.25% over the shown frequency range.

The attenuation constant $\alpha = -\mathcal{I}m\{k_z\}$ is shown in Fig. 8. The attenuation consists of an attenuation caused by dielectric losses in the $LaAlO_3$ substrate with $\tan\delta = 8.3 \cdot 10^{-5}$ at 10 GHz and an attenuation caused by normally conducting electrons in the $YBa_2Cu_3O_{7-x}$ superconductor. At the given miniature geometry the conductor losses predominate in spite of the use of superconductive material. The attenuation constant, α, increases very strongly ($\alpha \sim f^2$) in the shown frequency range.

Fig. 9 presents the horizontal distribution of the H_x component at the upper boundary of superconductor layer II. In the superconductor zones (regions 2 and 4) this is equivalent to the horizontal distribution of the longitudinal current, whereas in the gap zone (region 3) it corresponds to the longitudinal electric field component, E_z. The shape of the shown distribution does not vary over frequency.

The results for this high-T_c superconducting coplanar transmission line are now compared with a normally conducting transmission line made with gold conductors with the same geometry as above. The substrate material is also $LaAlO_3$. The material parameters for gold are

relative dielectric constant $\epsilon_{r2,4} = 0$;
normal conductivity (300 K) $\sigma_{2,4} = 4.51 \cdot 10^7$ S/m;
London penetration depth $\lambda_{l2,4} \to \infty$.

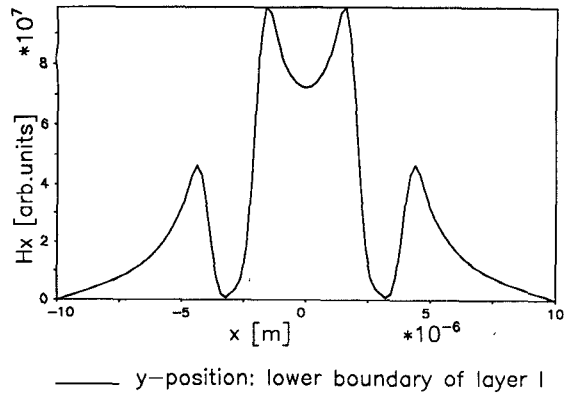

Fig. 9. Horizontal distribution of H_x component.

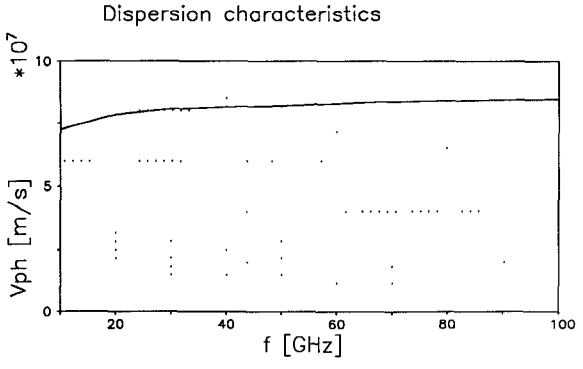

Fig. 10. Phase velocity (normal conducting case).

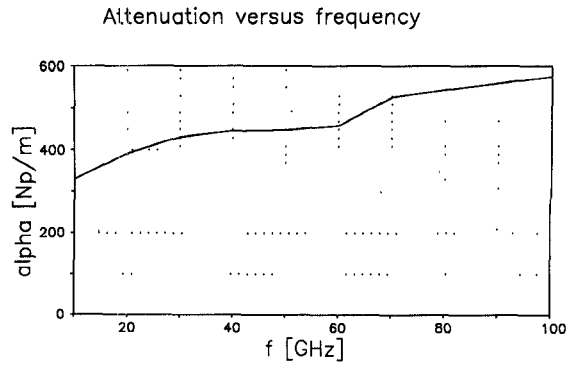

Fig. 11. Attenuation constant (normal conducting case).

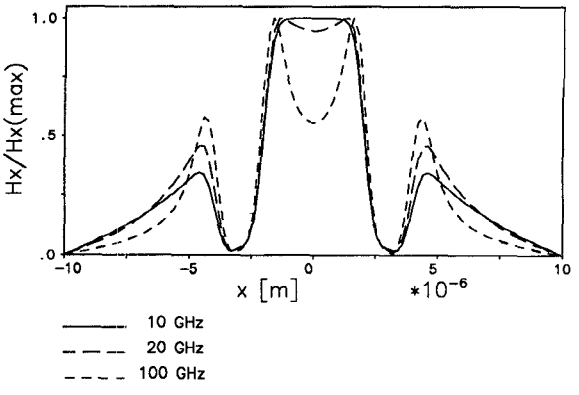

Fig. 12. Change of the horizontal distribution of the longitudinal current.

Fig. 10 shows the phase velocity, v_{ph}, versus frequency in the frequency range from 10 to 100 GHz. In contrast to the superconducting case, a significant variation can be observed.

The attenuation constant, α, is shown in Fig. 11. The attenuation consists of an attenuation caused by dielectric losses in the $LaAlO_3$ substrate and a strongly predominant attenuation caused by ohmic losses in the gold conductors. The constant increases slightly in the frequency range shown. This slight increase is caused mainly by the change in the horizontal distribution of the longitudinal current shown in Fig. 12. The horizontal current displacement increases with frequency. The solid line shows the distribution at 10 GHz, the line with long dashes at 20 GHz, and the line with short dashes at 100 GHz.

Comparing the two geometrically identical transmission lines, it can be said that the superconducting one is dispersion free and, especially in the lower frequency range, low in loss. At higher frequencies at about 100 GHz the low-loss advantage of the superconducting transmission line decreases rapidly because of the strong increase in the superconducting attenuation (see Fig. 8).

As already mentioned in Section IV, the coplanar transmission line structure as shown in Fig. 1 was also used for short-circuited $\lambda/2$ resonators. For resonator 1 [1], a coplanar waveguide transmission line resonator based on a $YBa_2Cu_3O_{7-x}$ thin film of 350 nm thickness on a MgO substrate, we calculate a Q_c value of 2350 according to a normal conductivity, σ, of $2.9 \cdot 10^6$ S/m and a London penetration depth, λ_l, of 300 nm at 77 K. The MgO substrate with its relative dielectric constant, ϵ_r, of 10 and its ohmic conductivity, σ, of $8 \cdot 10^{-4}$ S/m causes a dielectric Q value, Q_u, of 6790, which leads to an unloaded overall Q value, Q_u, of 1750. The measured Q_u value is, by comparison, 1300. For resonator 2 [2], on a $LaAlO_3$ substrate with a relative dielectric constant of 24 and a conductivity, σ, of $1.1 \cdot 10^{-3}$ S/m, which leads to the better dielectric Q value, Q_d, of 8120, we calculate a conductive Q value, Q_c, of 9100 according to a normal conductivity, σ, of $8.2 \cdot 10^5$ S/m and a London penetration depth, λ_l, of 300 nm. The resulting overall Q value, Q_u, is 4290, compared with a measured value of 3850 ± 180.

Table I presents data and results for both resonators [5]. The results show that, for the given geometry, the substrate losses are in the range of the superconductor losses that with resonator 2 they even become the limiting effect.

TABLE I

	Resonator 1	Resonator 2
Width of conductor strip $2w$	100 μm	74 μm
Gap width g	50 μm	46 μm
Superconductor thickness s	350 nm	280 nm
Substrate thickness d	1 mm	0.5 mm
Resonator length	7 mm	7 mm
Resonance frequency	8.8 GHz	6.5 GHz
σ superconductor (at 77 K)	$2.9 \cdot 10^6$ S/m	$8.2 \cdot 10^5$ S/m
λ_l superconductor (at 77 K)	300 nm	300 nm
ϵ_r substrate	10	24
σ substrate	$8 \cdot 10^{-4}$ S/m	$1.1 \cdot 10^{-3}$ S/m
Q_u measured	1300	3850 ± 180
Q_u calculated	1750	4290
Q_c calculated	2350	9100
Q_d calculated	6790	8120

VI. Conclusion

We have investigated a coplanar transmission line structure for use with superconductive material. A full-wave analysis has been performed by a partial wave synthesis and the electromagnetic field has been evaluated inside the superconducting regions as well. A miniaturized transmission line geometry with conductor width in the range of a few μm has been considered and compared with the normally conducting case. Attenuation and propagation behavior are shown in the frequency range up to 100 GHz as well as some field distributions. The superconducting transmission line has been proved to be not only low in loss but also nearly dispersion free up to 100 GHz. Finally the Q values of high-T_c coplanar waveguide resonators that have been produced are calculated and separated into Q values according to superconductor and substrate losses, Q_c and Q_d, respectively. At the given geometry in the range of a 100 μm conductor width the superconductor losses are so small that the substrate losses may become the limiting effect.

References

[1] A. A. Valenzuela and P. Russer, "High-Q coplanar transmission line resonator of $YBa_2Cu_3O_{7-x}$ on MgO," *Appl. Phys. Lett.*, vol. 55, pp. 1029–1031, 1989.

[2] A. A. Valenzuela, B. Daalmanns, and B. Roas, "High-Q coplanar transmission line resonator of $YBa_2Cu_3O_{7-x}$ on $LaAlO_3$," *Electron. Lett.*, vol. 25, pp. 1435–1436, 1989.

[3] E. B. Eckholm and S. W. McKnight, "Attenuation and dispersion for high-T_c superconducting microstrip lines," *IEEE Trans. Microwave Theory Tech.*, vol. 38, pp. 387–395, 1990.

[4] W. Heinrich, "Die Wellenausbreitung auf FET-Elektroden und ihr Einfluß auf das Übertragungsverhalten eines MESFET," dissertation, TH Darmstadt, 1987, Darmstadt, Germany, VDI-Verlag, 1987.

[5] J. Kessler, R. Dill, P. Russer, and A. A. Valenzuela, "Analyse von koplanaren Resonatoren aus hochtemperatur-supraleitenden Dünnfilmen," *Kleinheubacher Berichte*, vol. 34, pp. 161–170, 1991.

[6] M. Tinkham, *Introduction to Superconductivity*. New York: McGraw-Hill, 1975.

[7] F. J. Harris, "On the use of windows for harmonic analysis with the discrete Fourier transform," *IEEE Trans. Microwave Theory Tech.*, vol. MTT-26, pp. 51–83, 1978.

[8] H. Chaloupka, "High-temperature superconductors—A material for miniaturized or high-performance microwave components," *Frequenz*, vol. 44, pp. 141–144, 1990.

[9] R. W. Simon, *et al.*, "Low-loss substrate for epitaxial growth of high-temperature superconductor thin films," *Appl. Phys. Lett.*, vol. 53, pp. 2677–2679, 1988.

[10] J. Kessler, R. Dill, P. Russer, and A. A. Valenzuela, "Property calculations of a superconducting coplanar waveguide resonator," in *Proc. 20th European Microwave Conf.*, 1990, pp. 798–803.

[11] K.-S. Kong, H.-Y. Lee, and T. Itoh, "Analysis of the superconducting coplanar waveguide," in *Proc. 20th European Microwave Conf.*, 1990, pp. 792–797.

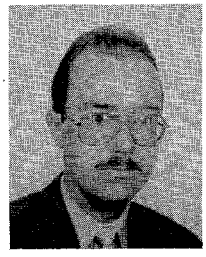

Jochen Kessler was born in Munich, Germany, in 1964. He received the Dipl. Ing. degree in electrical engineering from the Technical University of Munich, Germany, in 1988. Since then, he has been studying toward the Dr. Ing. degree in electrical engineering. His research deals with electromagnetic field theory and high-T_c superconductivity.

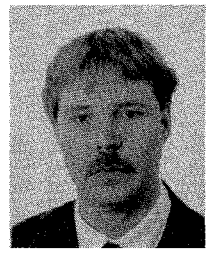

Roland Dill was born in Grossostheim, Germany, in 1956. He received the Dipl. Ing. and Dr. Ing. degrees in electrical engineering from the University of Darmstadt, Germany, in 1982 and 1987, respectively.

In 1982 he joined the Institute of High Frequency Techniques at the University of Darmstadt, where he did theoretical and experimental work on microwave antennas. Since 1987, he has been with Siemens, AG, Corporate Research and Development, Munich, where he is developing SAW devices and passive HTSC components for analog signal processing.

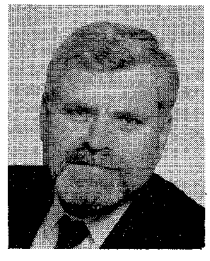

Peter Russer (SM'81) was born in Vienna, Austria, in 1943. He received the Dipl. Ing. degree in 1967 and the Dr. techn. degree in 1971, both in electrical engineering and both from the Technische Universität, Vienna, Austria.

From 1968 to 1971, he was an Assistant Professor at the Technische Universität, Vienna. In 1971 he joined the Research Institute of AEG-Telefunken in Ulm, where he worked on fiber-optic communication, high-speed solid-state electronic circuits, laser modulation, and fiber-optic gyroscopes. In 1979 he was a corecipient of the NTG award. Since 1981 he has held the chair of Hochfrequenztechnik at the Technische Universität München, Germany. His current research interests are microwave circuits, electromagnetic fields, statistical noise analysis of microwave circuits, methods for computer-aided design of microwave circuits, integrated microwave and millimeter-wave circuits, microwave oscillators, and microwave applications of superconductors.

Dr. Russer is the author of numerous scientific papers in these fields. He is a member of the German Informationstechnische Gesellschaft and of the Austrian and German Physical Societies. In 1990 he was a Visiting Professor at the University of Ottawa.